

See discussions, stats, and author profiles for this publication at: <https://www.researchgate.net/publication/231394077>

Excited states of s-indacene

ARTICLE *in* THE JOURNAL OF PHYSICAL CHEMISTRY · JANUARY 1995

Impact Factor: 2.78 · DOI: 10.1021/j100001a016

CITATIONS

14

READS

16

4 AUTHORS, INCLUDING:



[Leonardo Angeloni](#)

University of Florence

47 PUBLICATIONS 679 CITATIONS

[SEE PROFILE](#)

Excited States of *s*-Indacene

C. Gellini, L. Angeloni, and P. R. Salvi*

Laboratorio di Spettroscopia Molecolare, Dipartimento di Chimica, Università di Firenze,
via Gino Capponi 9, 50121 Firenze, Italy

G. Marconi

Istituto FRAE del CNR, via P. Gobetti 101, 40129 Bologna, Italy

Received: May 27, 1994; In Final Form: September 21, 1994^o

The electronic properties of 1,3,5,7-tetra-*tert*-butyl-*s*-indacene (TTBI), the stable derivative of antiaromatic *s*-indacene, have been studied via absorption and resonance Raman spectroscopy at low temperature. The two strongest absorption regions, at \approx 550 and 320 nm, show Franck-Condon structures suggesting change of excited-state geometry with respect to S_0 . Large enhancement factors have been measured for the most active Raman modes when the excitation frequency goes through the S_2 vibronic structure. By means of semiempirical QCFF-PI calculations ground- and excited-state optimized geometries and vibrational frequencies have been obtained for a quantitative estimate of vibronic Franck-Condon activities in the S_2 and S_6 states. The effect of normal-mode rotation in the excited state (Duschinsky effect) and alkyl substitution on the electronic and resonance Raman spectra of TTBI is discussed.

Introduction

Antiaromatic molecules are defined, as opposed to aromatic systems, in terms of the $4n$ ($n = 1, 2, 3, \dots$) π electrons of their planar conjugated cyclic structure.^{1,2} The ground-state structure of antiaromatic systems is usually described in terms of a localized arrangement of the ring electron density, roughly corresponding to alternating single and double C-C bonds, as it results from MO calculations for a number of such molecules.³⁻⁶ Excited states have received less attention. An important point of discussion on these states is their degree of antiaromaticity or, in other words, to what extent the excitation to virtual MO's changes the π -electron density over the ring. The stable indacene derivative, 1,3,5,7-tetra-*tert*-butyl-*s*-indacene (TTBI, see Figure 1), may be considered a convenient test case. TTBI shows a series of well separated one-photon absorptions ranging from the near-infrared to the UV with clear Franck-Condon profiles.^{7,8} In addition, the strong S_2 state, occurring around 550 nm, may be studied also by resonance Raman scattering. Probing the excited states with one-photon and/or resonance Raman techniques gives the basic answer to the problem. If S_n ($n \geq 1$) has an equilibrium structure different from that of S_0 , vibrational modes inducing the structural change will preferentially contribute to the Franck-Condon intensity.

In this paper we wish to report on the electronic absorption of TTBI up to 250 nm at low temperature and on the resonance Raman enhancement of totally symmetric modes following excitation into the S_2 state. Spectroscopic data are discussed and compared with results from semiempirical methods of calculation, widely used to estimate excited-state properties. In this respect the π -electron Hamiltonian with inclusion of a quantum mechanical force field (QCFF-PI)^{9,10} has been shown to describe correctly ground- and excited-state properties of a large number of conjugated and aromatic molecules¹¹⁻¹⁴ and has been already applied to the calculation of the ground-state normal modes of TTBI.⁶ By means of this method the Franck-Condon and Raman intensities have been calculated, in good agreement with experimental data. On the whole, our theoretical

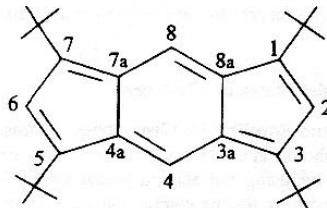


Figure 1. Molecular structure of 1,3,5,7-tetra-*tert*-butyl-*s*-indacene (TTBI).

estimates indicate that bond alternation disappears almost completely in the lowest active (S_2 and S_6) electronic states of TTBI.

Experimental Section

TTBI was kindly supplied by Prof. Hafner (Technische Universität Darmstadt, Darmstadt, Germany) and used without further purification. Experimental details about the spectroscopic measurements of TTBI have been already reported.^{6,8} TTBI solutions in a 7:3 isopentane-ether mixture were kept under vacuum in 1 mm quartz cells and quickly transferred in a low-temperature cryostat. Because of these precautions, the TTBI degradation due to air and thermal sensitivity¹⁵ was eliminated, and no signal decrease noticed during the experiments. All the experiments were carried out with freshly prepared solutions. At low temperatures, below the freezing point of the solvent mixture, the solution becomes glassy and completely transparent to the radiation. The background absorption signal is therefore small and this allows to rely on the full dynamic range of the spectrometer detection system. On the other hand, due to the random orientation of the TTBI molecules in the glassy matrix,^{16,17} all the bands are inhomogeneously broadened, making difficult the observation of the fine vibronic structure of the absorption spectrum. No other appropriate solvent was found to grow a TTBI-doped single crystal, and even under a low freezing rate a polycrystalline sample was obtained. In these conditions the spectral bandwidth

^o Abstract published in Advance ACS Abstracts, November 15, 1994.

is larger than for TTBI in the isopentane–ether solution. In addition, the polycrystalline samples scatter strongly the incident beam thus reducing the detection capabilities.

The absorption spectra on the two main-band systems, at ≈ 550 and 320 nm, respectively, were taken on a Cary 5 spectrometer operating with a resolution (≈ 10 cm $^{-1}$ in the first case and ≈ 30 cm $^{-1}$ in the second) much smaller than the experimental bandwidths. The spectra were measured at 77 and 15 K. At this later temperature the optical quality of the sample kept on being excellent, with no apparent internal cracking, providing the freezing rate was moderately low. Due to the strong absorption of the two electronic transitions, solute concentrations $\approx 10^{-5}$ M were used. Raman spectra of glassy TTBI solutions were measured at 77 K with excitation in the wavelength region 600 – 538 nm, in preresonance and resonance conditions with respect to S_2 , with two different experimental arrangements. In the first, the dye laser (rhodamine 6G, 600 – 566 nm; fluorescein 27, 566 – 544 nm) is pumped by a Nd:YAG mode-locked laser and, in the second, by a continuous-wave Ar $^+$ laser to reach, with fluorescein 27, 538 nm. The laser power was kept constant at ≈ 10 mW, and no damage was noticed on the sample. The Raman apparatus is standard, consisting of a double Jobin-Yvon monochromator operating at ≈ 2 cm $^{-1}$ resolution, a cooled PMT, a photon-counting detection system and a PC for data processing. TTBI concentrations ranging from 10^{-4} to 10^{-6} M, according to the excitation wavelength with respect to the (0–0) $S_0 \rightarrow S_2$ transition, were used.

Excited Singlet States of *s*-Indacene

Energies and Equilibrium Geometries. In this section the lowest one-photon active states of *s*-indacene are discussed theoretically by using the semiempirical QCFF-PI Hamiltonian.^{9,10} According to this calculation method, σ bonds and nonbonded interactions are considered by empirical potential functions, while the full SCF procedure is applied to π electrons. The ground-state equilibrium structure of *s*-indacene is found to have C_{2h} symmetry with peripheral bonds alternating in length (1.385 and 1.45 Å, on the average) and longer inter-ring bonds 7a–4a, 8a–3a. These data have been compared with ab initio values. In a past report,⁶ the short CC bond was found to increase from 1.33 to 1.356 Å changing the basis set from STO-3G to DZV. In this study we have found that the structural parameters of *s*-indacene depend also on multiconfigurational effects. The multiconfiguration self-consistent field (MCSCF) calculation for the ground state with the HONDO program¹⁸ and using the STO-3G basis set shows that also doubly excited configurations (HOMO, HOMO) \rightarrow (LUMO, LUMO) and (HOMO – 1, HOMO) \rightarrow (LUMO, LUMO + 2) are important for this state. Due to this, short CC bonds increase by ≈ 0.02 Å. The results of calculation, reported in Table 1, do not compare satisfactorily with X-ray diffraction data on TTBI^{4,19} which show that the ring structure has effective D_{2h} structure and no bond alternation. In early reports^{4,20} it was proposed that substitution at symmetry-equivalent positions may decrease the bond alternation of the parent molecule. On the contrary, quite recently it was reported²¹ that calculated ab initio data on *s*-indacene may be reconciled with experiment at a level of the MO theory beyond standard MCSCF procedure, that is including the dynamical electron correlation in a multireference scheme of second-order many-body perturbation theory.²² According to this result, *s*-indacene itself is an almost delocalized electron system with D_{2h} symmetry in the ground state. However, despite of the limitations of the QCFF-PI results, it may be seen from Table 1 that the difference between “double” and “single”

TABLE 1: Optimized Bond Lengths (Å) of *s*-Indacene as a Function of the MO Calculation and Experimental Values from X-ray Diffraction Data

	STO-3G ^a	STO-3G/MCSCF	DZV ^a	QCFF/PI	exp ^b
a	1.485	1.488	1.470	1.461	1.438
b	1.329	1.351	1.356	1.384	1.406
c	1.486	1.488	1.474	1.451	1.408
d	1.337	1.361	1.360	1.390	1.434
e	1.472	1.470	1.453	1.445	1.395
f	1.331	1.329	1.350	1.375	1.442
g	1.488	1.489	1.470	1.479	1.440

^a From ref 6. ^b From ref 19.

TABLE 2: Calculated Energies E and E' (eV) and Oscillator Strengths f of the Lowest Excited States of *s*-Indacene, According to QCFF-PI Calculations^a

	E	f	E'	E_{obs}	f_{obs}
$S_1(A_g)$	1.34			1.15	
$S_2(B_u)$	2.50	0.48	2.41	2.25	0.14
$S_3(B_u)$	3.72	0.25	3.62	2.72	0.001
$S_4(A_g)$	3.88				
$S_5(A_g)$	4.14				
$S_6(B_u)$	4.78	1.85	4.67	4.00	0.24
$S_7(A_g)$	5.47				
$S_8(B_u)$	6.07	0.085			
$S_9(A_g)$	6.14				
$S_{10}(A_g)$	6.31				

^a E , E' : vertical transition energies $S_0 \rightarrow S_n$ and $S_n \rightarrow S_0$ starting from the minimum of the S_0 and S_n potential surfaces, respectively; obs, observed values for TTBI.

bonds is considerably reduced with respect to previous ab initio analyses⁶ and that all the calculated bond lengths shift in the correct direction closer to the experimental values. In addition, it should be noted that the S_0 set of data will be considered in connection with the corresponding excited-state parameters derived from the same semiempirical procedure. The internal consistency may therefore justify its use in the following vibronic calculations.

The transition energies and oscillator strengths at the S_0 and excited-state (S_n) equilibrium structures using the whole $\pi\pi^*$ space in a singly-excited configuration interaction (SECI) are reported in Table 2. Comparison with observed data^{7,8} and previous CNDO results⁷ may be considered, on the whole, satisfactory. However, sizeable deviations from experiment occur in the case of the S_3 and S_6 states, particularly with reference to the oscillator strength values. Confirmed are, along with a previous calculation,⁷ the symmetry-forbiddenness of S_1 and the large energy gap between S_1 and S_2 . This latter point is related to the $S_2 \rightarrow S_0$ fluorescence of TTBI.^{7,8}

The optimized equilibrium structures of *s*-indacene in the S_2 , S_3 , and S_6 states are reported in Table 3. Large changes of the CC bond lengths are calculated in all three cases. Bond alternation almost disappears in S_2 and S_6 . The S_3 state, on the contrary, still retains C_{2h} symmetry. The inter-ring CC bonds decrease in S_2 and S_3 while are unchanged in S_6 . As a consequence, S_6 acquires a π -electron density largely delocalized over the peripheral ring, somehow similar to that of ground-state cyclododecahexane, the parent alternant hydrocarbon of *s*-indacene.²³

Vibrational Frequencies. The calculated frequencies of 15 a_g modes (the C–H stretchings are excluded) in S_0 and in the lowest B_u states (S_2 , S_3 , and S_6) are reported in Table 4. The

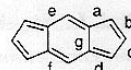


TABLE 3: Optimized Bond Lengths (\AA) of *s*-Indacene, According to QCFF-PI Calculations, in S_0 , S_2 , S_3 , and S_6 States

	S_0	S_2	S_3	S_6
a	1.461	1.441	1.421	1.409
b	1.384	1.418	1.432	1.431
c	1.451	1.414	1.403	1.424
d	1.390	1.445	1.445	1.416
e	1.445	1.413	1.424	1.422
f	1.375	1.416	1.454	1.430
g	1.479	1.449	1.435	1.479

TABLE 4: Calculated a_g Frequencies (cm^{-1}) of *s*-Indacene (Except C—H Stretchings) in S_0 and S_2 , S_3 , S_6 Excited States, According to QCFF-PI Calculations

	S_0			
calc	exp ^a	S_2	S_3	S_6
1650	1640	1597	1600	1597
1586	1589	1595	1578	1563
1519	1516	1477	1492	1497
1460		1453	1438	1431
1398	1382	1361	1369	1366
1334	1292	1340	1325	1338
1224		1232	1223	1228
1183		1183	1176	1203
1095	1119	1086	1087	1087
1064	1013	1081	1073	1070
846	813	856	859	841
785		791	787	779
661		657	656	656
500		497	491	492
447		446	440	444

^a From ref 6.

comparison with observed ground-state values of the Raman spectrum presents some difficulties, given that the experimental data refer to TTBI. It has been pointed out⁶ that assuming small coupling between the butyl and indacene moieties, the TTBI vibrations may be classified, in a first approximation, of butyl (B) or indacene (I) parentage. The criterion works well for CC-(I) stretches and CCH(I) bendings, calculated in the ranges 1650–1500 and 1400–1300 cm^{-1} and well separated from the CC(B) stretches (1500–1400 cm^{-1} range). As lower energy vibrations are considered, B—I coupling becomes more efficient and modes of mixed character are calculated. Below 400 cm^{-1} , the Raman modes have been assigned to the butyl group. Having in mind these considerations, the listed experimental frequencies of Table 4 have been reasonably interpreted as mostly due to displacements located on I.

Most of the a_g frequencies remain essentially unaltered going from the ground to the excited states. A small frequency decrease occurs only for the CC stretching modes, in agreement with the observation that the π -electron density is perturbed following excitation to higher MO's. This point has some importance in the calculation of Franck-Condon profiles as it suggests the occurrence of Duschinsky rotation among a_g modes, i.e., the rotation of excited-state CC normal coordinates with respect to ground-state modes.

Results

Electronic Absorption. The experimental absorption spectra of TTBI at 15 K in the regions 18 000–24 000 and 32 000–36 000 cm^{-1} are shown in Figures 2 and 3. They are assigned,

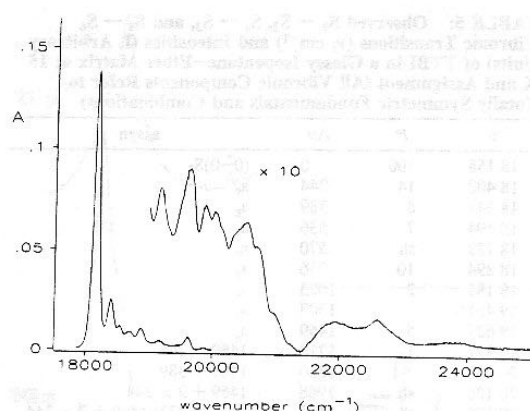


Figure 2. Absorption spectrum of TTBI 10^{-5} M in isopentane/ether solution at 15 K in the 18 000–24 000 cm^{-1} region.

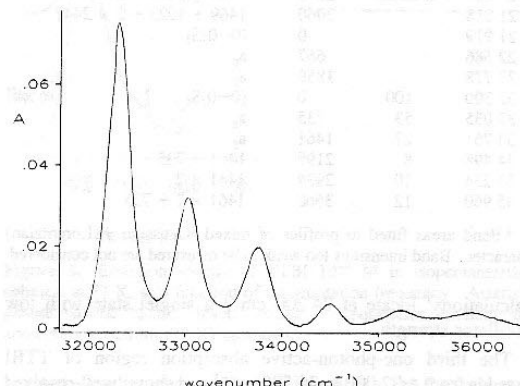


Figure 3. Absorption spectrum of TTBI 10^{-5} M in isopentane/ether solution at 15 K in the 32 000–36 000 cm^{-1} region.

according to the calculations of Table 2, to the $S_0 \rightarrow S_2$ and $S_0 \rightarrow S_6$ electronic transitions.

The S_2 state has been extensively investigated in previous reports because of its fluorescence properties^{7,8} and as a probe of the conformational isomers of TTBI.⁸ The $S_0 \rightarrow S_2$ transition is allowed ($f = 0.14$). The (0–0) band has maximum at 18 158 cm^{-1} and, due to the random orientation of the TTBI molecules in the glassy matrix, a profile with Gaussian character and bandwidth $\Gamma(\text{fwhm})$ of $\approx 120 \text{ cm}^{-1}$. The dependence of Γ on temperature is quite modest, being $\Gamma \approx 130 \text{ cm}^{-1}$ at 77 K. In an attempt to evaluate the homogeneous contribution to bandwidth, we prepared solid solution (10^{-5} M) of TTBI in various solvents, including *n*-alkanes (up to *n*-dodecane), branched alkanes, cyclohexane, and 1-methylnaphthalene, at a very low freezing rate. It turned out, unfortunately, that none of them was a good host crystal for TTBI, as we obtained in all cases polycrystalline matrices. The difficulty is probably related to the size of the bulky *tert*-butyl substituents. The vibronic structure of the $S_0 \rightarrow S_2$ transition extends for $\approx 3000 \text{ cm}^{-1}$, as shown in Figure 2, and is assigned entirely to totally symmetric vibrations. Full details of the assignment are given in Table 5. The frequencies of all the a_g fundamentals active in S_2 are quite similar to the ground-state values.⁶ It is also seen from Figure 2 that, above 21 300 cm^{-1} , the spectrum shows two broad bands centered at 21 919 and 22 586 cm^{-1} with much larger bandwidths than those of the preceding peaks. This may be evidence of a new electronic state.²⁴ In effect, MO semiempirical

TABLE 5: Observed $S_0 \rightarrow S_2$, $S_0 \rightarrow S_3$, and $S_0 \rightarrow S_6$ Vibronic Transitions (ν , cm^{-1}) and Intensities (I , Arbitrary Units) of TTBI in a Glassy Isopentane-Ether Matrix at 15 K and Assignment (All Vibronic Components Refer to Totally Symmetric Fundamentals and Combinations)

ν	I^a	$\Delta\nu$	assgn
18 158	100	0	(0-0) S_2
18 402	14	244	a_g
18 547	8	389	a_g
18 694	7	536	a_g
18 728	sh	570	a_g
18 894	10	736	a_g
19 181	2	1023	a_g
19 461		1303	a_g
19 627	5	1469	a_g
19 871	1	1713	1469 + 244
20 018	<1	1860	1469 + 389
20 126	sh	1968	1469 + 2 × 244
20 350	sh	2192	1469 + 733; 1469 + 3 × 244
20 526	<1	2368	1469 + 2 × 244 + 389
20 693		2535	1469 + 1023
20 968		2810	1469 + 1023 + 244?
21 218		3060	1469 + 1023 + 2 × 244?
21 919	0		(0-0) S_3
22 586		667	a_g
23 778		1859	a_g
32 300	100	0	(0-0) S_6
33 035	53	735	a_g
33 761	27	1461	a_g
34 498	8	2198	1461 + 735
35 234	10	2934	1461 × 2
35 960	12	3660	1461 × 2 + 735

^a Band areas fitted to profiles of mixed (Gaussian + Lorentzian) character. Band intensities too weak to be measured are not considered.

calculations⁷ locate at 24 200 cm^{-1} a singlet state with low oscillator strength.

The third one-photon-active absorption region of TTBI extends from $\approx 32\ 000$ to $36\ 500\ \text{cm}^{-1}$ and shows well-resolved bands at 15 K, with origin at 32 300 cm^{-1} (see Figure 3 and Table 5). The bandwidth (fwhm) of the first four bands is almost constant, $\approx 320\ \text{cm}^{-1}$, more than twice that of (0-0) S_2 , while the last two components, much broader and weaker, have $\Gamma \approx 490$ and $760\ \text{cm}^{-1}$, respectively. Although the vibronic spacings may suggest a mode progression built on the 735 cm^{-1} mode (742 cm^{-1} , ground-state value⁶) no single Franck-Condon profile can fit all the observed intensities. The calculated Franck-Condon factors of the next section indicate that the experimental profile is due to several fundamental a_g modes.

Resonance Raman and Fluorescence Spectra from S_2 . The Raman spectrum of TTBI is expected to show resonance effects as the excitation frequency approaches the (S_0-S_2) origin and runs across the vibronic structure of the S_2 state. Preresonance Raman spectra of TTBI ($c = 6 \times 10^{-4}\ \text{M}$, isopentane/ether solution mixture, 77 K), exciting in the range 17 000–17 860 cm^{-1} (588–560 nm), are reported in Figure 4. It is apparent that peaks at 390, 572, 742 cm^{-1} and the band multiplet below 300 cm^{-1} are strongly enhanced with respect to the solvent bands, as the excitation frequency shifts upward. Evidence of this was already reported for crystalline TTBI.⁸ Since TTBI fluoresces from S_2 ,^{7,8} both fluorescence and Raman signals may be observed, in principle, scanning through the absorption profile. It is well-known^{25–29} that when molecules are resonantly driven by light, two types of emission may be seen, resonance Raman scattering and fluorescence. Experimentally, the first emission shifts with excitation frequency while the latter is observed at fixed frequency. The Raman bandwidth is determined by that of the excitation source, while the fluorescence bands may be as broad as those of the absorption

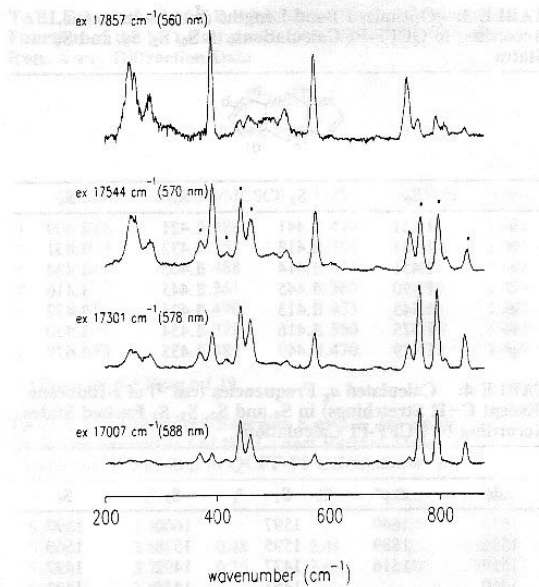


Figure 4. Preresonance Raman spectra of TTBI $6 \times 10^{-4}\ \text{M}$ in isopentane/ether solution at 77 K, as a function of the excitation frequency. Asterisks denote solvent bands.

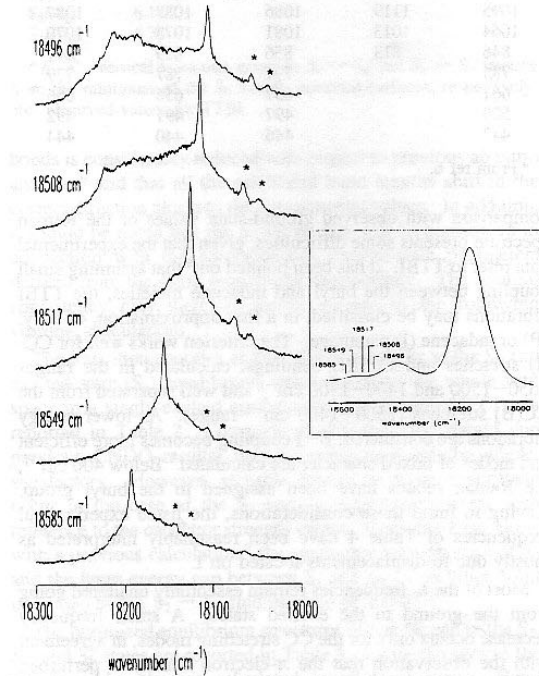


Figure 5. Emission spectra of TTBI $10^{-6}\ \text{M}$ in isopentane/ether solution at 77 K, as a function of the excitation frequency. Asterisks denote solvent bands. Inset: excitation frequencies scanning the absorption spectrum (77 K) as shown.

spectrum.²⁶ For a sufficiently monochromatic light source the two types of resonance are readily distinguishable.

The emission spectrum in the region of (0-0) S_2-S_0 , around 18 160 cm^{-1} , is shown in Figure 5, sweeping the excitation frequency the vibronic band (0-0) + 390 cm^{-1} . The Raman peak 390 cm^{-1} is easily identified as it shifts linearly with ν_{exc}

and has an estimated bandwidth $\approx 5 \text{ cm}^{-1}$, much narrower than that of the underlying emission. This latter broad emission is assigned, following previous considerations, as the origin band of the relaxed $S_2 \rightarrow S_0$ fluorescence. The fluorescence band has a peculiar behavior. As already noted,⁸ the TTBI molecules are randomly oriented into the glassy matrix, and as a consequence, the band is inhomogeneously broadened. Considering, for instance, the case of excitation on the band maximum, $18160 + 390 \text{ cm}^{-1}$, we observe a rather symmetrical fluorescence band, with bandwidth $\approx 85 \text{ cm}^{-1}$, on top of which stands the sharp 390 cm^{-1} Raman line (see Figure 5, second trace from the bottom). The homogeneous contribution (Γ_h) to bandwidth may be taken to be $\geq 2 \text{ cm}^{-1}$, from time-resolved femtosecond measurements on the S_2 state for TTBI in solution.⁷ Assuming, for the sake of simplicity, no Γ_h change for TTBI in the glassy matrix at 77 K, the inhomogeneous broadening determines almost completely the observed fluorescence bandwidth. For sufficiently monochromatic light sources as in our case different molecular distributions are excited whose Raman and fluorescence spectrum will be both shifted with ν_{exc} if the inhomogeneous broadening persists for a time longer than Γ_h^{-1} .²⁶ However, this is not actually the case, since when ν_{exc} lies on the wings of the absorption band (see Figure 5, first and last trace from the bottom), the fluorescence profile is found to be strongly asymmetric with respect to the Raman line. For intermediate excitation frequencies the fluorescence band broadens considerably, and two emissions are distinguished with some difficulty. Applying fitting procedures as discussed in detail later on, two fluorescence bands are found to give sizeable contributions to the observed profile, at a distance $\approx 70 \text{ cm}^{-1}$ each from the other (see Figure 8). These are assigned as emissions from different conformers of TTBI, resulting from hindered rotation of the butyl group around the $C_{\text{ring}}-C_{\text{but}}$ bond. In a previous paper⁶ it was pointed that the butyl group in 1-*tert*-butylindacene has two stable conformations, as a function of the torsion angle around C_1-C_{but} , one (A) with the equatorial $C_{\text{but}}-C_{\text{met}}$ bond looking at ring bond $C_2-\text{H}$ (and the other two $C_{\text{but}}-C_{\text{met}}$ bonds axially distributed above the below the indacene ring) and the second (B) with the equatorial bond pointing toward $C_8-\text{H}$. The energy difference between the two conformers (in favor of the former) is $\approx 350 \text{ cm}^{-1}$ in the ground state, according to 4-31G ab initio calculations.⁸ Therefore, the TTBI molecule may occur in 2⁴ conformers, among whom AAAA, the lowest in energy, is responsible of the absorption profile at 77 K. The AAAA conformer transforms to others, passing across the conformational energy barrier in the S_2 state. Evidence of the conformers has been already given.⁸ The energy difference between the strongest conformer emissions (18170 and 18090 cm^{-1})⁸ agrees well with the measured gap between the two fluorescence bands, $\approx 70 \text{ cm}^{-1}$.

For excitation energies below those considered so far and approaching the (0-0) band, the emission data cannot be divided sharply into Raman and fluorescence parts. Few representative spectra are shown in Figures 6 and 7. A single relatively symmetric band is observed up to $\nu_{\text{exc}} = 18363 \text{ cm}^{-1}$ whose maximum, at 245 cm^{-1} , shifts linearly with ν_{exc} . Looking back at the preresonance Raman data of Figure 4, it may be noted that the vibrational structure consisting of two closely lying bands, 245 and 255 cm^{-1} , and a third, 280 cm^{-1} , is almost completely washed out in the present situation. Apparently, the Raman and fluorescence signals have comparable bandwidths. When ν_{exc} approaches even further to the origin (see Figure 7), Raman and fluorescence contributions to the total emission may be more easily recognized. The fluorescence

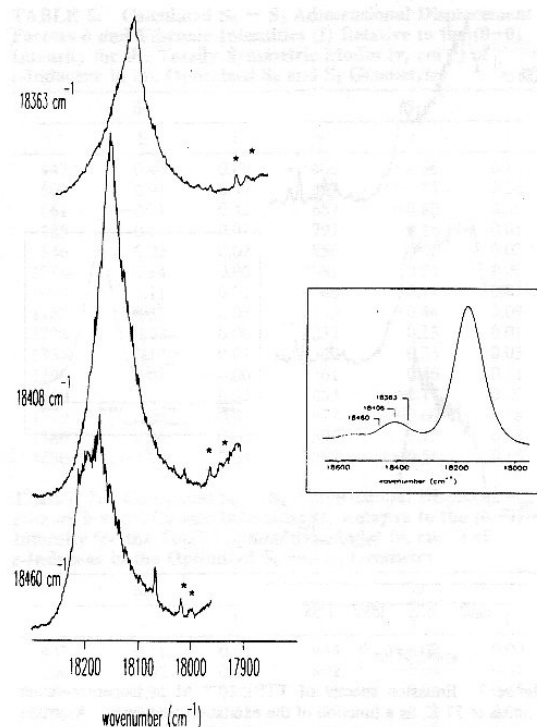


Figure 6. Emission spectra of TTBI 10^{-6} M in isopentane/ether solution at 77 K, as a function of the excitation frequency. Asterisks denote solvent bands. Inset: excitation frequencies scanning the absorption spectrum (77 K) as shown.

emission is relatively unshifted with respect to the Raman bands and broadens to a convolution of two, as in the case of Figure 5.

Resonance enhancement factors have been determined for the three Raman peaks, 390 , 572 , and 742 cm^{-1} . These are much narrower than those of the multiplet around 250 cm^{-1} , and their intensity may be therefore more easily deconvoluted from the total emission. The results are shown in Figures 9-11 for the three vibrations. The Raman intensity has been evaluated by a fitting procedure including all the bands in the region of the mode under consideration. Thus, with reference to Figure 5, $\nu_{\text{exc}} = 18496 \text{ cm}^{-1}$, seven bands, five of Raman and two of fluorescence origin, have been fitted to the observed profile. The result is shown in Figure 8. Band areas and heights are related to the solvent bands, 441 and 458 cm^{-1} . Due to their proximity to the 390 and 574 cm^{-1} Raman peaks, they take satisfactorily into account any reabsorption from the cell for emission frequencies falling in the region of the origin band. Following the same procedure, the intensity of the 742 cm^{-1} mode was compared to that of the nearby solvent bands, 763 and 795 cm^{-1} . All the enhancement factors are quite large for excitation near the electronic origin, ranging from ≈ 600 for the 390 cm^{-1} band to ≈ 400 for that at 742 cm^{-1} . The bandwidth of the excitation profile in all three cases coincides, within the experimental error, with the (0-0) absorption bandwidth.

Vibronic Intensities

Theory. The Franck-Condon structure of an allowed transition is determined by the factor $F_{v0} = \langle v_e | 0_g \rangle$, where $|0_g\rangle$ and $|v_e\rangle$ are vibrational wave functions relative to the ground and excited state, 0th and *v*th level, respectively. If normal

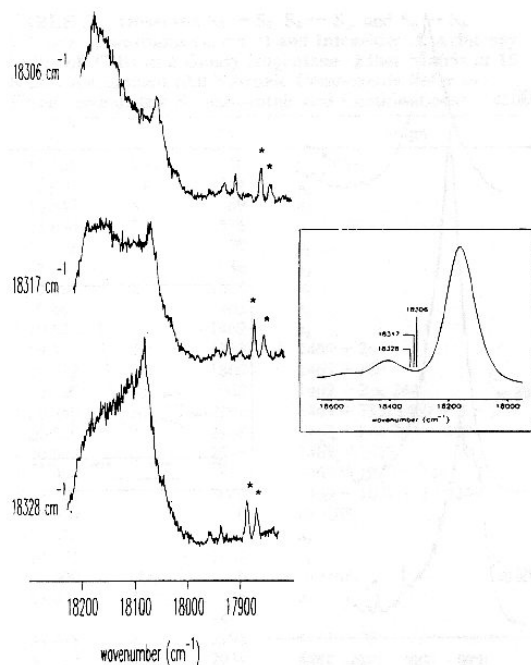


Figure 7. Emission spectra of TTBI 10^{-6} M in isopentane/ether solution at 77 K, as a function of the excitation frequency. Asterisks denote solvent bands. Inset: excitation frequencies scanning the absorption spectrum (77 K) as shown.

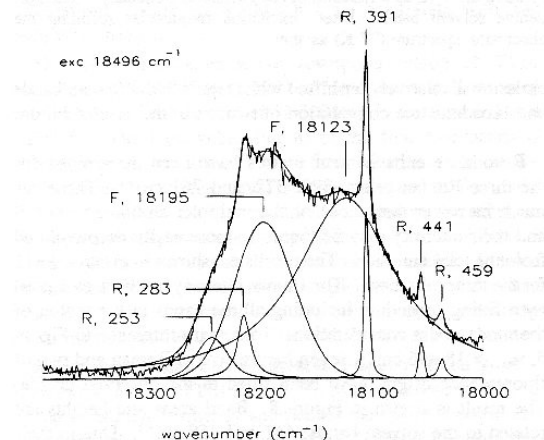


Figure 8. Experimental and calculated spectrum of TTBI 10^{-6} M (isopentane/ether solution, 77 K) for $v_{\text{exc}} = 18496 \text{ cm}^{-1}$. The calculated profile results from fitting with Raman bands (R, wavenumbers relative to v_{exc}) and fluorescence bands (F, absolute wavenumbers). The 441 and 449 cm^{-1} Raman bands are due to solvent.

mode mixing and frequency change upon electronic excitation are neglected, $F_{v,0}$ may be expressed in terms of only the displacement parameter b_i of the i th totally symmetric mode as¹¹

$$b_i = 0.172\omega_i^{1/2}(\mathbf{x}_e - \mathbf{x}_g)\mu^{1/2}\mathbf{L}_i = 0.172\omega_i^{1/2}\Delta_i \quad (1a)$$

where \mathbf{x}_g and \mathbf{x}_e are the $3n$ coordinates of the ground- and excited-state structure at equilibrium, μ the diagonal $3n \times 3n$ matrix of the atomic masses and \mathbf{L}_i ($=\mathbf{L}_{i,e} = \mathbf{L}_{i,g}$) the $3n$ -dimensional eigenvector for the i th mode (with frequency

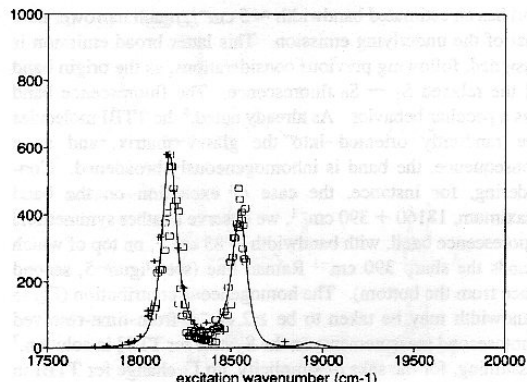


Figure 9. Experimental (crosses and squares, 390 cm^{-1} band, TTBI) and calculated (full line, 431 cm^{-1} mode, 1-*tert*-butyl-*s*-indacene) Raman enhancement factor F as a function of the excitation frequency.

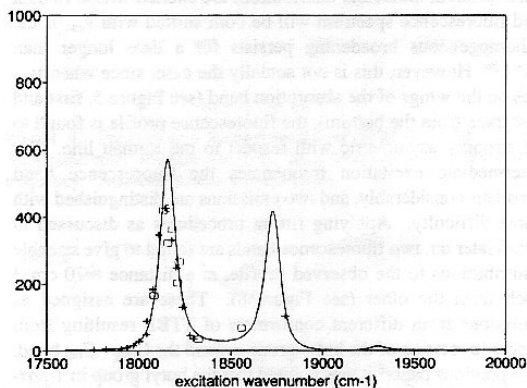


Figure 10. Experimental (crosses and squares, 572 cm^{-1} band, TTBI) and calculated (full line, 574 cm^{-1} mode, 1-*tert*-butyl-*s*-indacene) Raman enhancement factor F as a function of the excitation frequency.

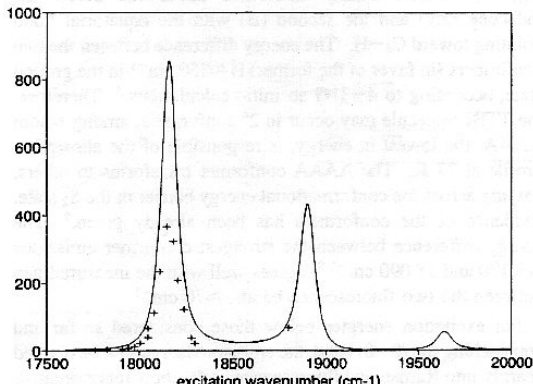


Figure 11. Experimental (crosses, 742 cm^{-1} band, TTBI) and calculated (full line, 689 cm^{-1} mode, 1-*tert*-butyl-*s*-indacene) Raman enhancement factor F as a function of the excitation frequency.

$\omega_i(\text{cm}^{-1})$, as a function of the mass-weighted Cartesian displacements. The relative Franck-Condon intensity $I_{v,0}/I_{00}$ is given, within the previous approximations, by

$$I_{v,0}/I_{00} = (F_{v,0}/F_{00})^2 = [(1/2)b_i^2]^{v_i}(1/v_i!) \quad (2)$$

Mode mixing (Duschinsky effect) is taken into account if

excited-state normal coordinates are considered. In this case $L_{i,e} \neq L_{i,g}$ and $\Delta_{i,g} \neq \Delta_{i,e}$. However, the two sets of normal coordinates, q_e and q_g , may be related through the equation³⁰

$$q_g = R q_e + D_g \quad (3)$$

where $R = L_g^{-1} L_e$ is the $(3n - 6) \times (3n - 6)$ Duschinsky matrix and $D_g = L_g^{-1} (x_e - x_g)$ the $(3n - 6)$ shift vector of the normal modes between the two electronic states. Accordingly, eq 1a transforms to

$$b_{i,e} = 0.172 \omega_{i,e}^{1/2} \Delta_{i,e} = 0.172 \omega_{i,e}^{1/2} \sum_j R_{ij} \Delta_{j,g} \quad (1b)$$

and eq 2 may be again used. In a Raman experiment the polarizability tensor

$$\alpha_{g0,gi} = \sum_{e=g} \sum_v \left[\frac{\mu_{g0,eu} \mu_{ev,gi}}{\omega_{ev} - \omega_{g0} - \omega_0 + (1/2)i\Gamma_{ev}} + \frac{\mu_{g0,ev} \mu_{ev,gi}}{\omega_{ev} - \omega_{gi} + \omega_0 + (1/2)i\Gamma_{ev}} \right] \quad (4a)$$

is considered for the vibrational transition $|0_g\rangle \rightarrow |j_g\rangle$.²⁵ Here $|e\rangle$ denotes the set of all vibronic states, with energy ω_{ev} , damping constant Γ_{ev} , and transition moment $\mu_{g0,eu}$, while ω_0 is the frequency of the incident light. When ω_0 is in near resonance with an allowed $g \rightarrow e$ transition (i.e., $\omega_0 \approx \omega_g$ and $\mu_{ge} \neq 0$) the second term of eq 4a may be neglected with respect to the first and the sum over the electronic states reduces to a single contribution. In the zeroth approximation, the vibronic transition moments may be expressed as a product of one electronic term, μ_{ge} , and a Franck-Condon factor and eq 4 results in³¹

$$\alpha_{g0,gi} = |\mu_{ge}|^2 \sum_v \frac{\langle 0_g | v_e \rangle \langle v_e | j_g \rangle}{(\omega_{ev} - \omega_{g0} - \omega_0 + (1/2)i\gamma_{ev})} \quad (4b)$$

This term is responsible for scattering of totally symmetric fundamentals. The Raman intensity is then proportional to $|\alpha_{g0,gi}|^2$ and therefore to the squared sum over vibronic states of the electronic level in near resonance. Also in this case the key quantities for calculation are Franck-Condon factors and may be found through eq 1a or 1b, according to the previous considerations. The explicit form of $\langle 0_g | v_e \rangle \langle v_e | j_g \rangle$, as a function of the displacement parameters, may be found elsewhere.³²

Franck-Condon Calculations. The adimensional displacement parameters b_i and $b_{i,e}$ of all the a_g modes (except C-H stretches) of *s*-indacene for the S_0/S_2 and S_0/S_6 pairs of states have been calculated according to eq 1a–1b and are reported in Tables 6 and 7, respectively, together with the relative Franck-Condon intensities.

On the whole, the calculated activity of all the a_g fundamentals in S_2 and S_6 is smaller than unity, in fair agreement with experimental results. However, in absence of mode mixing, for both transitions the vibronic lines are calculated more intense than observed. As to the $S_0 \rightarrow S_2$ transition, four modes, 500, 661, 1460, 1650 cm^{-1} (ground-state values), give vibronic intensities largely exceeding those of all other a_g modes. The Duschinsky matrix for the a_g vibrations in S_0 and S_2 , shown in Table 8, introduces a strong mixing of modes above 1000 cm^{-1} . The 1650 and 1460 cm^{-1} intensities are considerably redistributed upon excitation among the excited-state 1597, 1595, 1477,

TABLE 6: Calculated $S_0 \rightarrow S_2$ Adimensional Displacement Factors b and Vibronic Intensities (I) Relative to the (0–0) Intensity for the Totally Symmetric Modes (ν, cm^{-1}) of *s*-Indacene in the Optimized S_0 and S_2 Geometries

ν	S_0		S_2		I
	b	I	ν	b	
447	0.44	0.09	446	-0.56	0.16
500	0.91	0.42	497	-0.85	0.36
661	-0.91	0.42	657	-0.89	0.39
785	0.17	0.01	791	0.16	0.01
846	0.22	0.02	856	-0.26	0.03
1064	0.14	0.00	1081	0.04	0.00
1095	0.11	0.01	1086	0.14	0.01
1183	0.32	0.05	1183	-0.44	0.09
1224	0.04	0.00	1232	0.13	0.01
1334	0.12	0.01	1340	0.23	0.03
1398	0.07	0.00	1361	0.46	0.11
1460	1.02	0.52	1453	-0.77	0.29
1519	0.09	0.01	1477	-0.60	0.18
1586	0.06	0.00	1595	0.75	0.28
1650	-1.12	0.63	1597	-0.54	0.15

TABLE 7: Calculated $S_0 \rightarrow S_6$ Adimensional Displacement Factors b and Vibronic Intensities (I) Relative to the (0–0) Intensity for the Totally Symmetric Modes (ν, cm^{-1}) of *s*-Indacene in the Optimized S_0 and S_6 Geometry

ν	S_0		S_6		I
	b	I	ν	b	
447	0.11	0.01	444	-0.02	0.00
500	0.92	0.43	492	-0.94	0.44
661	-0.91	0.42	656	0.95	0.45
785	-0.17	0.01	779	0.12	0.01
846	-0.22	0.02	841	0.18	0.02
1064	-0.11	0.01	1070	-0.32	0.05
1095	0.20	0.02	1087	-0.17	0.02
1183	0.54	0.14	1203	-0.35	0.06
1224	0.14	0.01	1228	-0.17	0.02
1334	0.36	0.06	1338	0.16	0.01
1398	0.11	0.01	1366	-0.60	0.18
1460	0.48	0.11	1431	0.84	0.35
1519	0.74	0.27	1497	-0.24	0.03
1586	0.47	0.11	1563	0.49	0.12
1650	-1.14	0.65	1597	-0.92	0.42

1453, and 1361 cm^{-1} modes. The low-frequency modes, 500 and 661 cm^{-1} , however, have essentially unaltered frequencies and coordinates in S_2 and no appreciable intensity change results. The Duschinsky matrix for the a_g vibrations in S_0 and S_6 is reported in Table 9. The previous conclusions apply also to the $S_0 \rightarrow S_6$ vibronic structure.

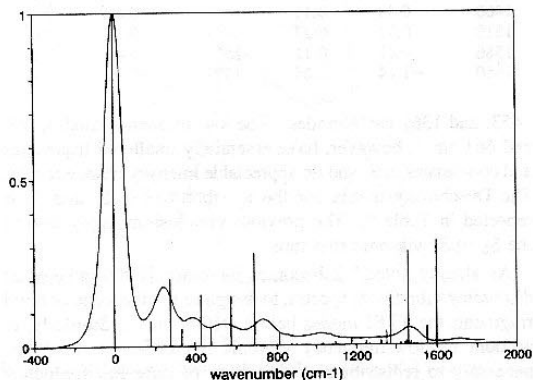
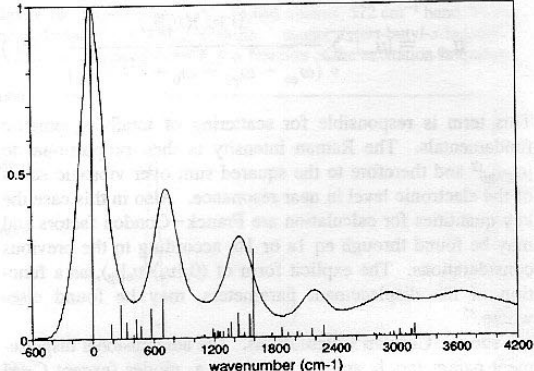
As already noted,⁶ it becomes increasingly difficult, when discussing vibrational spectra, to assign to the indacene or butyl fragments the TTBI modes below $\approx 1000 \text{ cm}^{-1}$. Similarly, to account for low-frequency vibronic intensities, it should be necessary to redistribute the intensity of pure low-frequency indacene modes over others due to coupling with *tert*-butyl substituents. Therefore QCFF-PI calculations were performed on the simplest derivative (1-*tert*-butylindacene), keeping in mind a model system of reduced size. The results for the $S_0 \rightarrow S_2$ and $S_0 \rightarrow S_6$ transitions, including Duschinsky mixing, are shown in Figures 12 and 13. The presence of *tert*-butyl groups does not change appreciably the C-C stretching intensity with respect to the corresponding *s*-indacene results. On the contrary, the coupling between displacements on the indacene ring and on the *tert*-butyl group gives comparable intensities for several modes in the range 400–800 cm^{-1} . In addition, the vibronic intensity of modes around 200 cm^{-1} , mostly located on the *tert*-butyl substituent, is predicted to be large, while being completely absent in the *s*-indacene case. Although the calculated data may depend in some extent also on the symmetry

TABLE 8: Duschinsky Matrix for the A_g Modes in the S_0 and S_2 States of *s*-Indacene (Only Coefficients Larger Than 0.05 Are Indicated)

	S_0														
S_2	1650	1586	1519	1460	1398	1334	1224	1183	1095	1064	846	785	661	500	447
1597	0.65	0.64	-0.37	0.11		0.08		0.07							
1595	-0.73	0.58	-0.32		0.11	-0.05									
1477	0.11	0.35	0.60	-0.55	0.40	-0.13	-0.07	0.08	-0.05	-0.06					
1453	0.10	-0.34	-0.62	-0.58	0.39	-0.05			0.06	-0.08					
1361			0.06	0.27	0.60	0.75	0.07			0.06					
1340	0.08			0.47	0.53	-0.56	-0.27	-0.33	0.53						
1232				0.10	0.15	-0.28	0.93	0.10	-0.06	0.09					
1183		0.10		-0.18	-0.10	0.20	0.22	-0.92			0.77	0.62			
1086				-0.07					0.07	0.62					
1081				0.56	0.09	0.05	0.12	0.07	0.62	-0.77					
856											-0.99	-0.17	0.06		
791											-0.19	0.98			
657											0.26	0.06	0.99		
497												0.05	-0.99	0.11	
446												-0.10	-0.99		

TABLE 9: Duschinsky Matrix for the A_g Modes in the S_0 and S_6 States (Only Coefficients Larger Than 0.05 Are Indicated)

	S_0														
S_6	1650	1586	1519	1460	1398	1334	1224	1183	1095	1064	846	785	661	500	447
1597	0.92	0.31	-0.16	0.09	-0.13	0.08									
1563	-0.31	0.86	-0.33	-0.08	0.15		-0.08	-0.05							
1497	-0.15	-0.22	-0.71	0.57	-0.27		-0.14	0.06							
1431	-0.12	0.32	0.57	0.55	-0.49			-0.07	0.07						
1366			-0.08	-0.33	-0.50	-0.79	-0.07	-0.09	-0.8	-0.05					
1338	-0.10		-0.13	-0.40	-0.62	0.50	0.30	0.33							
1228	-0.05		-0.05	-0.16	-0.17	0.30	-0.87	0.11	-0.09						
1203		0.07	-0.05	-0.17		0.19	0.36	-0.89	-0.07						
1087								-0.09	-0.79	-0.59					
1070		-0.05	-0.07	-0.10			-0.11	-0.07	-0.57	0.79					
841											-0.99	0.08			
779											-0.98	-0.06			
656											-0.07	-0.99			
492											0.06	-0.99	0.11		
444											-0.10	-0.99			

**Figure 12.** Observed (TTBI, 15 K) and calculated (fundamental a_g modes, 1-*tert*-butyl-*s*-indacene) Franck-Condon intensities of the $S_0 \rightarrow S_2$ transition. Calculations (vertical lines) include Duschinsky mixing in the excited state.**Figure 13.** Observed (TTBI, 15 K) and calculated (fundamental, overtone and combination a_g modes, 1-*tert*-butyl-*s*-indacene) Franck-Condon intensities of the $S_0 \rightarrow S_6$ transition. Calculations (vertical lines) include Duschinsky mixing in the excited state.

reduction of the model system, the substitution effect is clearly in the correct direction. The calculations were extended also to the $S_0 \rightarrow S_3$ transition of *s*-indacene. The vibronic intensities are more strongly affected by the change of the equilibrium structure than in the other two cases. In particular, the 1650 cm^{-1} C-C stretching vibration (ground-state value) has a calculated intensity larger than unity which redistributes almost exclusively into that of the 1578 cm^{-1} mode (S_3 value), considering the Duschinsky rotation. Plausibly, the calculated data cannot fit the experimental absorption data even with the

inclusion of substitutional effects. This gives a further, though indirect, indication about the correctness of the previous assignment.

The polarizability tensor (4b) may be calculated as a function of ν_{exc} for 1-*tert*-butylindacene, once the Franck-Condon factors are known. The sum over vibronic states have been extended up to $v = 3$, as the higher terms become negligibly small. The largest enhancements, squaring the vibronic sum, are calculated for the 431, 574, and 689 cm^{-1} modes. Associating the 431 cm^{-1} profile to that observed for the 390 cm^{-1} mode, we obtain

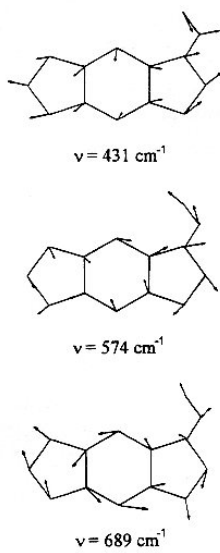


Figure 14. Vibrational modes $431, 574$, and 689 cm^{-1} of 1-*tert*-butyl-*s*-indacene with the largest calculated enhancement factors. For the sake of simplicity, only the C atoms of the indacene ring and the C atoms of the butyl group in the same plane are shown displaced.

the enhancement factors shown as full lines in Figures 9–11. In these calculations only one parameter has been adjusted, i.e., $\Gamma_{ev} = 130\text{ cm}^{-1}$, as observed for the $(0-0)S_0 \rightarrow S_2$ at 77 K. It should be noted that it is necessary to take into account substitution effects for a fair overall agreement with experiment, although symmetry reduction of the model system may influence again the results. The three a_g modes responsible for Raman enhancement are schematically shown in Figure 14. All of them are located on the indacene ring but in addition have large displacements on the C atoms of the tert-butyl groups. This may justify qualitatively the influence of the alkyl substitution on the Raman and absorption profiles.

Conclusions

In this paper the electronic properties of TTBI in the S_0 and S_6 states have been investigated by means of absorption and resonance Raman spectroscopy and compared with theoretical results obtained on the parent hydrocarbon, *s*-indacene, with semiempirical QCFF-PI calculations. There are two points of major interest in this study:

(1) Franck–Condon activity of S_2 and S_6 states and Raman profiles in resonance with S_2 show that large structural changes with respect to S_0 occur upon excitation.

(2) Normal-mode rotation and substituent effect cannot be neglected in the analysis of TTBI spectra.

Finally, it should be emphasized that *s*-indacene has a nonalternant arrangement of C atoms along the ring, in close similarity with azulene. Both molecules emit from S_2 due to the large S_2-S_1 energy gap. The search of other nonalternant systems of similar behavior as well as of a relationship between nonalternancy and energy level distribution are a research goal actively pursued in our laboratory at present time.

Acknowledgment. We thank Prof. Hafner for a generous supply of TTBI samples. This work was supported by the Italian Consiglio Nazionale delle Ricerche (CNR) under the P.F.-M.S.T.A. program.

References and Notes

- (1) Breslow, R. *Acc. Chem. Res.* **1973**, *6*, 393.
- (2) Garrat, P. J. *Aromaticity*; McGraw-Hill: London, 1971.
- (3) Elsaesser, T.; Laermr, F.; Kaiser, W.; Dick, B.; Niemeyer, M.; Lutke, W. *Chem. Phys.* **1988**, *126*, 405.
- (4) Hafner, K.; Stowasser, B.; Krimmer, H.-P.; Fischer, S.; Bohm, M.; Linder, H. J. *Angew. Chem., Int. Ed. Engl.* **1986**, *25*, 630.
- (5) Bischof, P.; Gleiter, R.; Hafner, K.; Knauer, K. H.; Spanget-Larsen, J.; Suss, H. U. *Chem. Ber.* **1978**, *111*, 932.
- (6) Gellini, C.; Cardini, G.; Salvi, P. R.; Marconi, G.; Hafner, K. *J. Phys. Chem.* **1993**, *97*, 1286.
- (7) Klann, R.; Bauerle, R. J.; Laermr, F.; Elsaesser, T.; Neimeyer, M.; Lutke, W. *Chem. Phys. Lett.* **1990**, *169*, 172.
- (8) Gellini, C.; Salvi, P. R.; Hafner, K. *J. Phys. Chem.* **1993**, *97*, 8152.
- (9) Warshel, A.; Karplus, M. *J. Am. Chem. Soc.* **1972**, *94*, 5612.
- (10) Warshel, A.; Levitt, M. *QCPE* **247**, Indiana University, 1974.
- (11) Zerpetto, F.; Zgierski, M. Z. *Chem. Phys.* **1986**, *110*, 421.
- (12) Zerpetto, F.; Zgierski, M. Z.; Orlandi, G.; Marconi, G. *J. Chem. Phys.* **1987**, *87*, 2505.
- (13) Orlandi, G.; Zerpetto, F. *Chem. Phys.* **1988**, *123*, 175.
- (14) Negri, F.; Zgierski, M. Z. *J. Chem. Phys.* **1992**, *97*, 7124.
- (15) Hafner, K. *Pure Appl. Chem.* **1982**, *54*, 939.
- (16) Albrecht, A. C. *J. Mol. Spectrosc.* **1961**, *6*, 84.
- (17) Russel, P. G.; Albrecht, A. C. *J. Chem. Phys.* **1964**, *41*, 2536.
- (18) Dupuis, M.; Farazdel, A. *HONDO-8 in MOTECC-91, Modern Techniques in Computational Chemistry*; Clementi, E., Ed.; ESCOM: Leiden, 1991.
- (19) Dunitz, J. D.; Kruger, C.; Ingartinger, H.; Maverick, E. F.; Wang, Y.; Nixdorf, M. *Angew. Chem., Int. Ed. Engl.* **1988**, *27*, 387.
- (20) Heilbronner, E.; Yang, Z. Z. *Angew. Chem., Int. Ed. Engl.* **1987**, *26*, 360.
- (21) Hertwig, R. H.; Holthausen, M. C.; Koch, W.; Maksic, Z. B. *Angew. Chem., Int. Ed. Engl.* **1994**, *33*, 1192.
- (22) Anderson, K.; Malmqvist, P.-A.; Roos, B. O.; Sadlej, A. J.; Wolinski, K. *J. Phys. Chem.* **1990**, *94*, 5483.
- (23) Nakajima, T.; Saijo, T.; Yamaguchi, H. *Tetrahedron* **1964**, *20*, 2119.
- (24) Hochstrasser, R. M.; Marzzacco, C. *J. Chem. Phys.* **1969**, *49*, 233.
- (25) Behringer, J. *In Raman Spectroscopy. Theory and Practice*; Szymanski, H. A., Ed.; Plenum Press: New York, 1967; Vol. 1, p 168.
- (26) Hochstrasser, R. M.; Novak, F. A. *Chem. Phys. Lett.* **1977**, *48*, 1.
- (27) Hochstrasser, R. M.; Novak, F. A. *Chem. Phys. Lett.* **1978**, *53*, 3.
- (28) Fujimura, Y.; Kono, H.; Nakajima, T.; Lin, S. H. *J. Chem. Phys.* **1981**, *75*, 99.
- (29) Hochstrasser, R. M.; Nyi, C. A. *J. Chem. Phys.* **1979**, *70*, 1112.
- (30) Zerpetto, F.; Zgierski, M. Z. *Chem. Phys.* **1988**, *127*, 17.
- (31) Tang, J.; Albrecht, A. C. *In Raman Spectroscopy. Theory and Practice*; Szymanski, H. A., Ed.; Plenum Press: New York, 1970; Vol. 2, p 33.
- (32) Siebrand, W.; Zgierski, M. Z. In *Excited States*; Lim, E. C., Ed.; Academic Press: New York, 1979; Vol. 4, p 1.